

Task-Oriented Data Synthesis and Control-Rectify Sampling for Remote Sensing Semantic Segmentation

Yunkai Yang¹, Yudong Zhang², Kunquan Zhang¹, Jinxiao Zhang², Xinying Chen³,
Haohuan Fu², Runmin Dong^{1*}

¹Sun Yat-Sen University

²Tsinghua University ³Beijing Institute of Technology

yangyk26@mail2.sysu.edu.cn, dongrm3@mail.sysu.edu.cn

Abstract

With the rapid progress of controllable generation, training data synthesis has become a promising way to expand labeled datasets and alleviate manual annotation in remote sensing (RS). However, the complexity of semantic mask control and the uncertainty of sampling quality often limit the utility of synthetic data in downstream semantic segmentation tasks. To address these challenges, we propose a task-oriented data synthesis framework (TODSynth), including a Multimodal Diffusion Transformer (MM-DiT) with unified triple attention and a plug-and-play sampling strategy guided by task feedback. Built upon the powerful DiT-based generative foundation model, we systematically evaluate different control schemes, showing that a text-image-mask joint attention scheme combined with full fine-tuning of the image and mask branches significantly enhances the effectiveness of RS semantic segmentation data synthesis, particularly in few-shot and complex-scene scenarios. Furthermore, we propose a control-rectify flow matching (CRFM) method, which dynamically adjusts sampling directions guided by semantic loss during the early high-plasticity stage, mitigating the instability of generated images and bridging the gap between synthetic data and downstream segmentation tasks. Extensive experiments demonstrate that our approach consistently outperforms state-of-the-art controllable generation methods, producing more stable and task-oriented synthetic data for RS semantic segmentation. The code is available at <https://github.com/Yunkai-Yang/crfm>.

1. Introduction

Semantic segmentation in remote sensing (RS) imagery plays a crucial role in land-use classification [23], environmental monitoring [4], and thematic mapping [20]. How-

ever, compared with natural image segmentation, RS semantic segmentation faces substantial challenges due to the complex diversity of land-cover types across spatial resolutions and regions, the difficulty in collecting samples of rare classes, and the requirement for domain-specific expertise. Building large-scale pixel-wise labeled datasets for RS tasks is therefore time-consuming and expensive [9]. Recently, with the rapid advancement of generative models, data synthesis has emerged as a promising alternative to alleviate annotation scarcity and enrich training data for downstream segmentation models [10, 28].

Early progress in text-to-image diffusion models [13, 15, 22, 31, 33] demonstrated remarkable capabilities in generating diverse and realistic samples for classification tasks. Controllable generation has further extended this paradigm to layout-to-image for object detection[38, 49] and mask-to-image for semantic segmentation [30, 39], as exemplified by ControlNet [53] and its variants [21, 32, 57]. The emergence of transformer-based architectures [13, 22, 31] such as Diffusion Transformers (DiTs) has significantly improved generation quality. These powerful pre-trained generation models, such as SDXL [33] and Stable Diffusion 3.5 [35], provide a strong foundation for synthetic data generation and have been widely adapted for natural scene image synthesis.

Despite the maturity of ControlNet-style conditioning mechanisms, effectively controlling DiT-based generative models remains an open challenge [12]. While some studies employ adapter-based modules to inject conditional information, cross-attention control often suffers from inefficient semantic utilization and potential modality conflicts. To mitigate these issues, methods such as CreateLayout [52] introduce siamese multimodal DiTs to decouple modalities and reduce interference. However, for RS imagery, the substantial domain gap between aerial and natural scenes, together with the absence of DiT models pre-trained on RS data, makes it highly uncertain to establish an effective

*Corresponding author

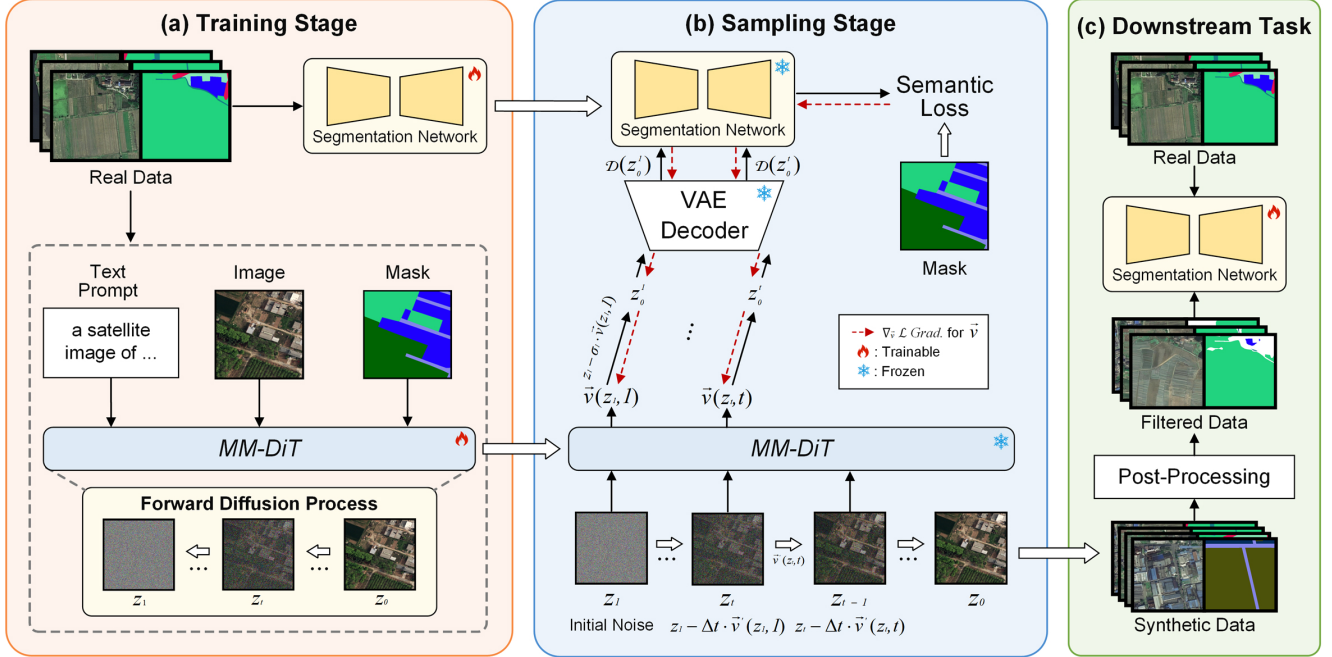


Figure 1. The overall workflow of the task-oriented data synthesis framework (TODSynth) consists of three stages: (a) Training stage using an MM-DiT generative model conditioned on text and mask. (b) Sampling stage with the proposed control-rectify flow matching (CRFM). (c) Downstream tasks trained on a combination of real and synthetic data.

mask-to-image control scheme.

In addition, the inherent stochasticity of the sampling process often leads to semantic drift and control deviation, resulting in unstable mask-conditioned generation and reduced effectiveness of synthetic data in downstream tasks. Recent studies typically adopt sample filtering strategies to directly select [40] or selectively utilize high-quality synthetic data [29]. For instance, FreeMask [48] introduces adaptive filtering and re-sampling to suppress noisy labels caused by inconsistencies between generated images and masks, while promoting the synthesis of more complex scenes. Such post-processing strategies practically retain the effective regions of synthetic data for downstream training. Similarly, EarthSynth [30] employs a rule-based CLIP scoring mechanism [2, 14] to evaluate image-object-background triplets and filter more informative samples for downstream tasks. Although these methods help reduce noise in synthetic datasets, they are inherently post-generation solutions and cannot fully resolve the intrinsic uncertainty of generation quality. In complex or few-shot scenarios, strict filtering may remove useful annotations and significantly degrade the performance of downstream tasks.

To address these limitations, we propose a task-oriented data synthesis framework that systematically examines mask-control strategies and introduces a control-rectify sampling method for RS semantic segmentation. We first compare different mask-to-image control schemes and ob-

serve that an appropriate DiT-based control design can markedly improve the effectiveness of synthetic data. In RS scenarios where fine-grained text descriptions are scarce, the text-image-mask joint attention scheme consistently outperforms both mask-adaptor and siamese MM-attention approaches.

Second, to mitigate the inherent uncertainty in sampling, we propose a control-rectify flow matching method, a plug-and-play sampling strategy guided by downstream task feedback. By leveraging the semantic loss signals from a pre-trained segmentation model, the sampler dynamically adjusts the sampling trajectory during the early high-plasticity stage, enabling in-process quality optimization. This improves the relevance and stability of synthetic data in complex and few-shot scenarios, rather than relying solely on post-processing filtering.

We conduct extensive experiments demonstrating that the proposed task-oriented data synthesis approach achieves OA/mIoU/mAcc improvements of 1.39%/4.14%/6.83% on FUSU-4k [51] and 1.60%/2.08%/2.22% on LoveDA-5k [43] compared to baseline. Our main contributions are summarized as follows:

- We introduce TODSynth, a task-oriented data synthesis framework that integrates architecture-level and sampling-level control to enhance the effectiveness of synthetic data for RS semantic segmentation.
- We propose a control-rectify flow matching (CRFM) method to mitigate generation uncertainty and enhance

the performance in complex and few-shot RS scenes. It is a task-feedback-guided sampling optimization strategy that leverages a pre-trained task network to refine generation without retraining the diffusion model.

- We conduct extensive experiments on two representative remote sensing semantic segmentation tasks, showing that the proposed TODSynth outperforms existing SOTA generation methods.

2. Related Work

2.1. Conditional Image Generation

Conditional image generation [27, 42, 46, 52, 53] aims to generate images under specific constraints such as layouts, masks, or text prompts. In this work, we mainly introduce layout-to-image and mask-to-image generation. ControlNet [53] achieves effective control by combining a frozen pre-trained diffusion backbone with a trainable copy through “zero convolution” layers, enabling guidance of the decoder under single or multiple conditions, such as depth maps, edges, or segmentation masks. Beyond this, adapter-based variants such as UniControl [46] enable flexible multi-condition fusion. Recent MM-DiT [13, 37, 45] explore different control strategies based on DiT architecture. For example, CreateLayout [52] introduces a siamese MM-DiT to decouple text and layout modalities, while EasyControl [54] and UniCombine [42] employ lightweight condition injection and use LoRA modules to improve training efficiency.

Synthesizing training data for remote sensing (RS) semantic segmentation [6, 10, 29] has gained increasing attention due to the scarcity of labeled data. SatSynth [41] explores joint generation of images and corresponding masks for satellite segmentation by training diffusion models from scratch. However, training diffusion models on small RS datasets often yields suboptimal results. To overcome this limitation, several RS generative foundation models have been developed, including DiffusionSat [16], EarthSynth [30], and TerraGen [39], which build upon Stable Diffusion (SD) v1.5 [1] and are trained on large RS datasets to enable controllable generation. Similarly, TISynth [10] introduces additional reference guidance to achieve transferable RS semantic segmentation data synthesis via joint reference-semantic fusion, also based on SD v1.5.

Despite these advances, major challenges remain due to the domain gap between natural and RS imagery, the limited availability of RS-specific DiT pre-trained models, and the uncertainty in effective DiT control strategies. In this work, we systematically explore mask-to-image control schemes for RS semantic segmentation and adopt MM-DiT with unified triple attention.

2.2. Training Data Synthesis for Downstream Tasks

Synthetic data has been widely employed to augment training datasets for downstream tasks such as semantic segmentation. Existing works [29] generally adopt uncertainty-aware segmentation approaches or sample filtering methods, e.g., adaptive filtering [48] and CLIP-based selection [30, 40]. While these methods are effective in reducing noise, they rely on post-processing and cannot resolve the intrinsic uncertainty of generation quality, particularly in complex or few-shot scenarios.

In related areas such as dataset distillation [8, 34, 44] and layout-to-image (L2I) generation [52, 58], some works attempt to improve synthetic data via distribution matching [17, 19] or trajectory matching [3, 11]. The training-free L2I method [5] apply marginal attention constraints to optimize latent features, enhancing spatial controllability and reducing semantic failures. However, these strategies are misaligned with semantic segmentation objectives, limiting their direct applicability.

Different from these approaches, we propose a control-rectify flow matching method to mitigate generation uncertainty and enhance the effectiveness of synthetic data for downstream tasks. Our method leverages semantic loss to dynamically adjust the sampling directions during the early, high-plasticity stage of generation. This strategy improves the effectiveness of generated data without directly modifying feature maps or constraining the distribution of synthetic samples, providing a task-oriented solution for robust data synthesis in RS semantic segmentation. Additional related work on inversion-free editing is provided in Appendix A.

3. Methodology

3.1. Preliminary

Flow-based generative models formulate data synthesis as a continuous transport from a base distribution to the target distribution. The evolution of a sample along a trajectory \mathbf{y}_t parameterized by $t \in [0, 1]$ is described by an ordinary differential equation (ODE):

$$\frac{d\mathbf{y}_t}{dt} = \mathbf{v}_\theta(\mathbf{y}_t, t), \quad (1)$$

where \mathbf{v}_θ denotes a learnable velocity field. Flow Matching (FM) [24] supervises the model with ideal transport velocities constructed between paired samples, enabling stable training without stochastic score matching. Rectified Flow (RF) [25] further simplifies this by assuming a linear trajectory between the endpoints:

$$\mathbf{z}_t = (1 - t)\mathbf{z}_0 + t\mathbf{z}_1, \quad (2)$$

with constant velocity $\mathbf{v}_\theta = \mathbf{z}_1 - \mathbf{z}_0$, allowing deterministic and efficient generation.

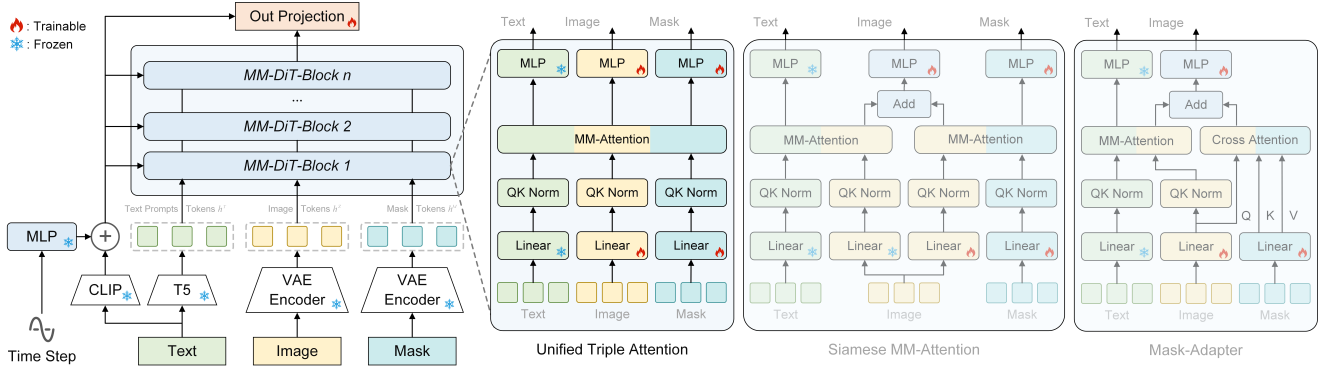


Figure 2. The architecture of MM-DiT with unified triple attention. For comparison, the mask-adapter and siamese MM-attention schemes are also illustrated.

3.2. The Overall Workflow of TODSynth

Due to the high cost of expanding RS datasets, we propose TODSynth, a training data synthesis framework designed to enhance the performance of downstream RS semantic segmentation models. Considering the challenges of fine-grained semantic control, we integrate architecture-level and sampling-level control strategies to improve the effectiveness of synthetic data. The overall workflow is illustrated in Fig. 1.

At the architecture level, to enhance mask-to-image control, we adopt the MM-DiT architecture combined with the pre-trained SD v3.5 model (Fig. 1(a)). To address semantic imbalance, global semantic information is embedded into the text prompt, which is combined with pixel-level mask guidance. A text–image–mask unified attention mechanism is employed to strengthen the model’s ability to generate complex scenes and few-shot categories. We further compare different DiT-based control strategies (Fig. 2), demonstrating that the text–image–mask joint attention scheme consistently outperforms both mask-adapter and siamese MM-attention approaches on this task.

Despite improvements at the architecture level, the stochastic nature of the generation trajectory can still cause deviations from the semantic mask constraints in certain regions, reducing the effectiveness of the synthesized data. To address this, we propose a sampling-level control strategy, namely Control-Rectify Flow Matching (CRFM) (Fig. 1(b)). During the high-plasticity early sampling stage, CRFM adjusts the trajectory by applying a rectification vector \mathbf{v}'_{rec} to the predicted velocity field. This vector is computed from the cross-entropy loss between early predictions and the ground-truth mask, enhancing the alignment of the generated samples with the semantic constraints and mitigating uncertainty in data synthesis.

Finally, the refined synthetic data is combined with real samples and used to train downstream semantic segmentation models (Fig. 1(c)).

3.3. Unified Triple Attention

Our work builds upon the SOTA MM-DiT architecture adopted by the SD v3.5 family. We focus on effectively incorporating semantic masks \mathbf{C}^m to achieve precise spatial control during image generation. MM-DiT performs multimodal fusion using a Unified Attention mechanism that processes the text sequence \mathbf{h}^t and image latent sequence \mathbf{h}^z jointly by concatenating their tokens:

$$\mathbf{h}_o^t, \mathbf{h}_o^z = \text{Attn}([\mathbf{h}^t, \mathbf{h}^z]), \quad (3)$$

where $[\cdot, \cdot]$ denotes length-wise concatenation. Each modality uses its own projection matrices ($\mathbf{W}_q, \mathbf{W}_k, \mathbf{W}_v$) to map features into the query, key, and value spaces. On this basis, we examine three mask-conditioning strategies: unified triple attention, siamese MM-attention, and mask-adapter.

Unified triple attention (Tri-attention) extends MM-DiT by adding a third modality stream for the mask sequence \mathbf{h}^m . Following the unified fusion principle, attention is computed over all three token sequences:

$$\begin{aligned} \mathbf{h}_o^t, \mathbf{h}_o^z, \mathbf{h}_o^m = \text{Attn}([\mathbf{h}^t \mathbf{W}_q^t, \mathbf{h}^z \mathbf{W}_q^z, \mathbf{h}^m \mathbf{W}_q^m], \\ [\mathbf{h}^t \mathbf{W}_k^t, \mathbf{h}^z \mathbf{W}_k^z, \mathbf{h}^m \mathbf{W}_k^m], \\ [\mathbf{h}^t \mathbf{W}_v^t, \mathbf{h}^z \mathbf{W}_v^z, \mathbf{h}^m \mathbf{W}_v^m]). \end{aligned} \quad (4)$$

Tri-attention integrates the mask stream directly, enabling crucial cross-modal interaction between the textual and mask modalities during the fusion process, allowing the semantic information encoded in the text to enhance the model’s understanding of the required spatial and semantic distribution.

We also evaluate the siamese MM-attention in L2I [52]. It processes text–image and mask–image interactions through two separate MM-attention blocks. Unlike L2I generation, the pure segmentation mask in M2I lacks localized textual descriptions, reducing semantic richness. Although the siamese design originally intended to mitigate token-length imbalance across modalities, this issue is less pro-

nounced in M2I due to the natural tokenization of the mask, diminishing the benefit of decoupled attention.

Mask-Adapter injects mask features into the image branch using a lightweight cross-attention module while keeping the MM-DiT backbone unchanged. Although computationally efficient, the mask information suffers from two limitations: 1) it is not directly fused with text embeddings, weakening the learning of global semantic information, especially in fine-grained and few-shot scenarios. 2) The mechanism only allows \mathbf{h}^z to query \mathbf{h}^m , meaning the mask representation remains static throughout the denoising process, restricting its adaptive refinement. These constraints limit the precision and controllability of the generated results.

Through the above analysis, we adopt the Tri-attention scheme and fully fine-tune both the image and mask branches, given the lack of DiT-based generative models pre-trained on diverse RS imagery.

3.4. Control-Rectify Flow Matching

Upon training a conditional generative flow model [24, 25], the inherent stochasticity of the trajectory and the imperfections in model prediction inevitably lead to generated images that, in certain regions, deviate from the semantic mask constraints during the inference process. Such conditional deviations often manifest in the early stages of the model’s generation, where small errors are rapidly amplified. Therefore, we propose the Control Rectify Flow Matching (CRFM) mechanism, enabling the timely correction of the velocity vector early in the flow trajectory, thereby ensuring the synthesized results adhere more faithfully to the target semantic distribution.

The original RF model predicts a constant vector field, defined simply as $\mathbf{v} = \mathbf{z}_1 - \mathbf{z}_0$. When incorporating the conditional controls \mathbf{C}^t and \mathbf{C}^m (text and semantic mask), the ideal vector field \mathbf{v}_Θ for the conditional flow trajectory retains this straight-line property. It can be formally expressed as:

$$\mathbf{v}_\Theta(\mathbf{z}_t, t, \mathbf{C}^t, \mathbf{C}^m) = \mathbf{z}_1 - \mathbf{z}_0. \quad (5)$$

This formulation implies that, ideally, at every time step t along the probabilistic path, the model’s predicted vector field remains the deterministic constant difference between the terminal data point \mathbf{z}_0 and the initial noise point \mathbf{z}_1 , irrespective of the current state \mathbf{z}_t .

Therefore, the generation process, which maps the initial noise sample \mathbf{z}_1 to the final data sample \mathbf{z}_0 , is described by solving the ODE via integration from $t = 1$ to $t = 0$:

$$\mathbf{z}_0 = \mathbf{z}_1 + \int_1^0 \mathbf{v}_\Theta(\mathbf{z}_t, t, \mathbf{C}^t, \mathbf{C}^m) dt. \quad (6)$$

In practical implementation, this continuous integration is typically approximated using numerical solvers, such as the

Euler method, which discretizes the process into N time steps. The iterative generation is then described by the following update rule:

$$\mathbf{z}_{t_{i-1}} = \mathbf{z}_{t_i} + \mathbf{v}_\Theta(\mathbf{z}_{t_i}, t_i, \mathbf{C}^t, \mathbf{C}^m) \cdot \Delta t, \quad (7)$$

where $\mathbf{z}_{t_N} = \mathbf{z}_1$ is the starting noise, and the final generated sample is $\mathbf{z}_{t_0} \approx \mathbf{z}_0$.

Assuming \mathbf{v}_Θ^T is the target velocity field that guides samples toward the data distribution, and \mathbf{v}_Θ^P is the learned velocity field predicted by the flow model, the residual vector \mathbf{v}_{res} can be calculated as the difference between the true and predicted fields:

$$\mathbf{v}_{\text{res}} = \mathbf{v}_\Theta^T - \mathbf{v}_\Theta^P. \quad (8)$$

We utilize this residual vector as the rectified vector field \mathbf{v}_{rec} . Consequently, the target velocity field can be decomposed and represented as:

$$\mathbf{v}_\Theta = \mathbf{v}_\Theta^P + \mathbf{v}_{\text{rec}}. \quad (9)$$

Theoretically, if we can accurately compute \mathbf{v}_{rec} at every step along the flow trajectory, then regardless of any inherent drift or deviation in the learned field, the final synthesized result will align well with the target data distribution.

Unlike standard data distributions, the conditional data distribution $q(\mathbf{z}_0 | (\mathbf{C}^t, \mathbf{C}^m))$ represents the mapping from the initial latent noise $\mathbf{z}_1 \sim p(\mathbf{z})$ to the target latent state \mathbf{z}_0 , conditioned on textual prompts \mathbf{C}^t and semantic masks \mathbf{C}^m . Generating samples from this conditional distribution requires the flow model to produce a velocity field that strictly respects the specified conditions, particularly the spatial constraints imposed by \mathbf{C}^m . Although the unified triple attention scheme is designed to produce an appropriate conditional vector field based on the input modalities, the stochasticity inherent in the initial latent noise and the complexity of the mask constraints inevitably lead to deviations in the generated semantics. This motivates the need for an early, targeted trajectory correction mechanism to enforce strict adherence to the conditions throughout the flow.

The proposed CRFM mechanism introduces an innovative, targeted gradient-based correction at the early stages of the generation trajectory. Specifically, CRFM first generates a pre-synthesized prediction of the final sample, \mathbf{x}_0^t , using the current state, \mathbf{z}_0 and the predicted velocity field \mathbf{v}^P :

$$\mathbf{z}_0^t = \mathbf{z}_t - \sigma_t \mathbf{v}^P(\mathbf{z}_t, t, \mathbf{C}^t, \mathbf{C}^m), \quad (10)$$

$$\mathbf{x}_0^t = \mathcal{D}(\mathbf{z}_0^t), \quad (11)$$

where \mathcal{D} denotes the VAE decoder that maps the latent space to the image space. Here, \mathbf{z}_0^t is the predicted latent representation of the final sample, and \mathbf{x}_0^t serves as the input to a pre-trained segmentation network \mathcal{S} . The output of this network is then used to compute a Cross-Entropy loss against the ground-truth semantic mask \mathbf{C}^m :

$$\nabla_{v^P} = \mathcal{L}_{CE}(\mathcal{S}(\mathbf{x}_0^t), \mathbf{C}^m). \quad (12)$$

The resulting gradient is back-propagated to produce the predicted rectified vector field, denoted as \mathbf{v}'_{rec} , which estimates the theoretically required residual vector \mathbf{v}_{rec} . This correction is incorporated to update the predicted velocity field:

$$\mathbf{v}'(\mathbf{z}_t, t, \mathbf{C}^t, \mathbf{C}^m) = \mathbf{v}^P(\mathbf{z}_t, t, \mathbf{C}^t, \mathbf{C}^m) + \alpha \mathbf{v}'_{\text{rec}}, \quad (13)$$

where α is a tunable scalar that controls the strength of the correction applied at each step. This process effectively adjusts the predicted velocity vector \mathbf{v}^P during the critical early steps, ensuring stricter adherence to the specified conditions throughout the generation. The proposed CRFM differs fundamentally from previous methods in its optimization target. Instead of performing gradient optimization directly on the latent state \mathbf{z}_t [5], we focus on rectifying the underlying velocity vector field \mathbf{v}_{Θ} , which indirectly updates \mathbf{z}_t through ODE integration.

Based on the above theoretical analysis, we also validated this intuition experimentally. We found that direct optimization of \mathbf{z}_t using the gradient of downstream tasks leads to mode collapse, where the generative model fails to capture the full diversity of the target distribution and instead converges to a limited subset of samples, resulting in ineffective synthetic data. By contrast, optimizing the underlying velocity field provides stable, continuous corrections along the trajectory, thereby effectively mitigating mode collapse.

Moreover, it is important to note that we apply this task-guided loss gradient only during the early stages of sampling. On one hand, the early stage exhibits high stochasticity, making it more amenable to trajectory adjustment. On the other hand, pre-trained segmentation models inherently contain prediction errors. These errors, although present, can still provide useful guidance for coarse adjustments at early steps. Applying corrections too late in the trajectory, however, could amplify these errors, making the sampling process overly dependent on the segmentation model. This may generate adversarial-like perturbations that deviate from the normal image distribution and degrade synthetic quality. Therefore, the proposed CRFM adjusts the directions of velocity field only in the early step, effectively reducing uncertainty in data synthesis and ensuring that the generated results adhere more faithfully to the target semantic distribution.

3.5. Implementation Details

Our TODSynth model leverages the MM-DiT [13] architecture, building upon the foundational SD v3.5 [35] framework. The model is trained at a 512×512 resolution. Optimization is performed using the AdamW optimizer, setting the learning rate to $\eta = 1 \times 10^{-5}$ and the weight decay to 0.01. For post-processing, image synthesis for each semantic mask involves redefining and fixing a sequence of

random seeds. A subsequent filtering step ensured that the synthesized images either resulted in a minimum of three distinct classes or preserved those classes containing only a few samples. Our models are trained for 200,000 steps on 8 NVIDIA RTX 4090 GPUs.

Our semantic segmentation approach is implemented using the MMSegmentation framework [26]. For fair comparison and robust training, we adopt the standard data augmentation techniques integrated within MMSegmentation. These techniques include basic transformations (random crop and random flip) and the comprehensive PhotoMetricDistortion, which sequentially applies a range of photometric adjustments, such as random brightness, random contrast, random saturation, and random hue.

4. Experiment

4.1. Datasets and Evaluation

FUSU. FUSU [51] is a high-resolution aerial land-cover dataset originally developed for change detection research. The imagery is sourced from Google Earth with a spatial resolution of approximately 0.2–0.5 m. FUSU provides fine-grained annotations covering 17 land-cover categories (e.g., residential, industrial, cropland, inland water, wetland, park, commercial land, greenbelt, service land, etc.). Following the setting in TISynth [10], we use a 4,000-sample subset of FUSU (denoted as FUSU-4k) and adopt the T1 image-mask pairs cropped to 512×512 pixels for training and evaluation.

LoveDA. LoveDA [43] is a domain-adaptive semantic segmentation benchmark consisting of 5,987 images with 0.3 m resolution and a spatial size of $1,024 \times 1,024$ pixels. It includes six semantic classes: building, road, water, barren, forest, and agriculture. In this work, we consider the rural-to-urban setting, using 3,274 rural images for training and 2,713 urban images for testing.

Evaluation metrics. Semantic segmentation performance is measured using Overall Accuracy (OA), Mean Intersection over Union (mIoU), and Mean Accuracy (mAcc). Image synthesis quality is evaluated using Fréchet Inception Distance (FID).

4.2. Comparison Results

We compare TODSynth with SOTA training data synthesis methods on two RS semantic segmentation datasets. The comparison methods include four UNet-based controllable generators (i.e., Freestyle [47], FreeMask [48], ControlNet [53], and SynthEarth [30]) and a MM-DiT-based controllable generation method (i.e., SD v3.5 with Tri-attention).

For a fair comparison, all methods except SynthEarth are fine-tuned on the same RS datasets. SynthEarth, as a large-scale generative foundation model trained on extensive RS

Table 1. Quantitative comparison with different training data synthesis methods (%). We report segmentation performance, the use of post-processing filters, and the ratio of synthetic to real training data for each method.

Method	Post-processing	Syn/Real volume	FUSU-4k			LOVEDA-5k		
			OA	mIoU	mAcc	OA	mIoU	mAcc
Baseline [56]	-	-	74.27	45.27	56.44	78.22	64.04	78.71
Freestyle [47]	×	×10	73.49	44.99	57.75	78.59	64.10	78.77
Controlnet [55] (SD v1.5)	×	×10	73.85	45.13	56.77	78.24	63.89	79.42
FreeMask [48]	FM	×5	74.23	45.83	56.29	79.26	64.93	79.06
SynthEarth* [30]	CLIP Score	×5	75.35	47.53	58.91	78.87	64.07	78.00
SD v3.5 [35]	FM	×3	75.41	48.57	61.67	79.72	65.45	79.91
Ours	FM	×3	75.66	49.41	63.27	79.82	66.12	80.93

*SynthEarth is a unified generative model that can be directly used for inference.

Table 2. Comparison of different control strategies on FUSU-4k.

Method	FUSU-4k		
	OA	mIoU	mAcc
Controlnet [55] (SD v1.5)	73.85	45.13	56.77
Mask-adapter	74.94	47.41	59.62
Siamese MM-attention	74.94	48.46	61.44
Tri-Attention	75.41	48.57	61.67

imagery and supporting training-free controllable generation, is directly used to synthesize RS segmentation data without additional tuning. All downstream semantic segmentation experiments use the same model architecture.

To isolate the contribution of the proposed CRFM, we evaluate SD v3.5 using the same architecture and post-processing filter as TODSynth. Therefore, the presence or absence of CRFM is the only difference. Table 1 summarizes distinctions among all methods, including post-processing strategies, the ratio of synthetic to real training samples, and segmentation performance on FUSU-4k and LoveDA. Fully supervised training on real data is used as the baseline.

Across both datasets, TODSynth consistently achieves the best performance. Compared to the supervised baseline trained on real data, TODSynth improves OA/mIoU/mAcc by 1.39%/4.14%/6.83% on FUSU-4k and 1.60%/2.08%/2.22% on LoveDA. Moreover, MM-DiT-based models exhibit stronger controllability compared with UNet-based generators, even when the SynthEarth is a RS generative foundation model. This advantage is particularly evident on FUSU, which contains 17 diverse land-cover categories.

Comparing TODSynth with SD v3.5 under identical architecture and post-processing settings, our CRFM achieves an improvement of 0.84%/1.6% mIoU/mAcc on FUSU-4k and 0.67%/1.02% mIoU/mAcc on LoveDA by dynamically adjusting the sampling trajectory. This demonstrates the ef-

fectiveness of the proposed sampling-level control.

Furthermore, TODSynth achieve superior performance with fewer synthetic samples compared to methods requiring larger synthetic datasets, highlighting its practical utility.

4.3. Ablation Study

We conduct the ablation study on the FUSU dataset. All experiments use the same post-processing strategy and downstream semantic segmentation implementation.

For DiT-based controllable generation, we compare three control strategies: Unified Triple Attention (Tri-Attention), Siamese MM-Attention, and Mask-Adapter, using ControlNet (SD v1.5) as the baseline. As shown in Table 2, Tri-Attention consistently outperforms both Siamese MM-Attention and Mask-Adapter. The Mask-Adapter, while efficient, provides limited control because it does not fuse text and mask embeddings and keeps mask features static, restricting precision and adaptability. In contrast, MM-DiT-based methods achieve better performance, and Tri-Attention achieves the best results with a concise implementation. We therefore adopt Tri-Attention in this work.

For post-processing of synthetic data, current approaches can be grouped into image-level filtering, e.g., CLIP-based methods like Earthsynth [30] and SDS [40], and pixel-level filtering, e.g., Freemask [48] and TISynth [10]. We compare these two types of post-processing filters, as well as the combination with our proposed CRFM. As shown in Table 3, pixel-level filtering significantly improves downstream performance, particularly in mIoU and mAcc, due to its finer-grained region selection. Incorporating CRFM into the pixel-level filter further boosts performance (0.84%/1.60% mIoU/mAcc on FUSU), demonstrating its effectiveness in complex and few-shot scenarios.

4.4. Discussion

We further analyze the effectiveness and sensitivity of CRFM. We conduct extensive experiments using different

Table 3. Comparison of different post-processing strategies on FUSU-4k.

Experiment	FreeMask Filter [48]	CLIP Score Filter [30]	CRFM	OA	mIoU	mAcc
Exp1	×	✓	×	74.78	46.69	58.08
Exp2	✓	×	×	75.41	48.57	61.67
Exp3 (Ours)	✓	×	✓	75.66	49.41	63.27

Table 4. Performance of CRFM with different sampling steps and CRFM steps on FUSU-4k.

Method	OA	mIoU	mAcc	FID
step=23, CRFM=0	75.41	48.57	61.67	35.85
step=23, CRFM=2	75.79	48.80	61.05	34.86
step=23, CRFM=4	75.66	49.41	63.27	38.65
step=23, CRFM=6	75.71	48.74	61.30	66.95
step=18, CRFM=0	75.53	47.81	59.32	40.23
step=18, CRFM=2	75.86	47.99	59.46	38.94
step=18, CRFM=4	76.24	48.93	60.54	57.01
step=18, CRFM=6	76.02	49.57	62.19	86.69
step=13, CRFM=0	75.02	46.86	59.44	49.53
step=13, CRFM=2	75.73	48.29	59.99	48.61
step=13, CRFM=4	76.08	49.04	62.05	81.90
step=13, CRFM=6	76.19	49.09	62.50	132.92

sampling steps and CRFM steps to test its sensitivity to the sampling step and empirical usage.

As discussed in the Methodology section, early adjustment of the sampling trajectory helps reduce the gap between synthetic data and downstream tasks, mitigating the uncertainty in synthetic data. First, with the standard sampling step of 23, we apply CRFM starting from the first step, using 2, 4, and 6 CRFM steps. CRFM=0 represents the baseline without CRFM. As shown in Table 4, we observe that the effectiveness of synthetic data for downstream tasks and its quality initially improve and then decline as CRFM steps increase. This is because early-stage randomness allows easier trajectory adjustment, but excessive adjustment becomes constrained by the capabilities of the pre-trained segmentation model. Over-adjustment also generates adversarial-like samples that deviate from the natural image distribution, causing a deterioration in FID. Therefore, CRFM is sensitive to the number of adjustment steps and the pre-trained segmentation model. In practice, applying CRFM for about the first four steps balances downstream performance and synthetic data quality.

Next, we test shorter sampling steps with 18 and 13 steps, again starting CRFM from the first step with 2, 4, and 6 adjustment steps. We observe the same trend: synthetic data quality initially improves with more CRFM steps but declines if over-adjusted, particularly at 6 steps, where downstream performance may still increase but FID drops

significantly due to adversarial-like artifacts. Thus, when reducing the number of sampling steps, we also reduce the number of CRFM steps. Additional sensitivity analyses regarding the pre-trained segmentation model appear in the Appendix B.

Based on these analyses, we summarize the limitations and future directions of this study:

The first issue is CRFM sensitivity. CRFM is sensitive to the sampling step and the pre-trained segmentation model. Applying it for a small number of early steps is the most stable approach. It also requires a sufficiently capable pre-trained segmentation model; with very limited data, the model does not provide effective guidance, reducing CRFM’s effectiveness. We will explore more robust pre-trained models, such as RS foundation models, to improve the effective of evaluation and sampling stability.

The second issue is synthetic data diversity and cross-domain performance. Currently, we do not leverage a strong RS generative foundation model or external RS reference data, which limits the diversity of synthetic samples. Future work explores incorporating additional information to enhance the effectiveness of synthetic data for downstream tasks.

5. Conclusion

In this paper, we propose a training data synthesis framework for RS semantic segmentation that integrates an MM-DiT architecture with task-guided sampling. We systematically evaluate different mask-to-image control schemes for this task. To enhance control over mask boundaries and semantics in the synthesized data, we adopt a unified triple attention mechanism within MM-DiT control blocks, improving the interaction between text, image, and mask. Furthermore, we introduce the control-rectify flow matching method, guided by semantic loss, to dynamically adjust sampling directions during the early, high-plasticity stage. This approach mitigates the intrinsic uncertainty of generation quality, thereby improving the utility of synthesized data for downstream semantic segmentation tasks. Extensive experiments demonstrate the strong control capabilities of our framework in mask-guided synthesis and task-guided sampling, surpassing SOTA approaches for semantic segmentation data synthesis. This work shows that task-oriented data synthesis can substantially enhance the effectiveness of synthetic data for downstream applications.

References

- [1] Stability AI, RunwayML, and LAION. Stable Diffusion v1-5 Model Card, 2022. 3
- [2] Romain Beaumont. Laion-5b: A new era of open large-scale multi-modal datasets. *Laion. ai*, 2022. 2
- [3] George Cazenavette, Tongzhou Wang, Antonio Torralba, Alexei A Efros, and Jun-Yan Zhu. Dataset distillation by matching training trajectories. In *Proceedings of the IEEE/CVF Conference on Computer Vision and Pattern Recognition*, pages 4750–4759, 2022. 3
- [4] Bin Chen, Shengbiao Wu, Yimeng Song, Chris Webster, Bing Xu, and Peng Gong. Contrasting inequality in human exposure to greenspace between cities of global north and global south. *Nature Communications*, 13(1):4636, 2022. 1
- [5] Huancheng Chen, Jingtao Li, Weiming Zhuang, Haris Vikalo, and Lingjuan Lyu. Training-free layout-to-image generation with marginal attention constraints, 2025. 3, 6
- [6] Yuhua Chen, Wen Li, Xiaoran Chen, and Luc Van Gool. Learning semantic segmentation from synthetic data: A geometrically guided input-output adaptation approach. In *Proceedings of the IEEE/CVF conference on computer vision and pattern recognition*, pages 1841–1850, 2019. 3
- [7] Bowen Cheng, Ishan Misra, Alexander G Schwing, Alexander Kirillov, and Rohit Girdhar. Masked-attention mask transformer for universal image segmentation. In *Proceedings of the IEEE/CVF conference on computer vision and pattern recognition*, pages 1290–1299, 2022. 2
- [8] Justin Cui, Ruochen Wang, Si Si, and Cho-Jui Hsieh. Scaling up dataset distillation to imagenet-1k with constant memory. In *International Conference on Machine Learning*, pages 6565–6590. PMLR, 2023. 3
- [9] Runmin Dong, Lichao Mou, Mengxuan Chen, Weijia Li, Xin-Yi Tong, Shuai Yuan, Lixian Zhang, Juepeng Zheng, Xiaoxiang Zhu, and Haohuan Fu. Large-scale land cover mapping with fine-grained classes via class-aware semi-supervised semantic segmentation. In *Proceedings of the IEEE/CVF International Conference on Computer Vision*, pages 16783–16793, 2023. 1
- [10] Runmin Dong, Shuai Yuan, Litong Feng, Jinxiao Zhang, Weijia Li, Mengxuan Chen, Bin Luo, Wayne Zhang, and Haohuan Fu. Transferable image synthesis for remote sensing semantic segmentation via joint reference-semantic fusion. *Information Fusion*, 127:103839, 2026. 1, 3, 6, 7, 2
- [11] Jiawei Du, Yidi Jiang, Vincent YF Tan, Joey Tianyi Zhou, and Haizhou Li. Minimizing the accumulated trajectory error to improve dataset distillation. In *Proceedings of the IEEE/CVF conference on computer vision and pattern recognition*, pages 3749–3758, 2023. 3
- [12] Zheng-Peng Duan, Jiawei Zhang, Xin Jin, Ziheng Zhang, Zheng Xiong, Dongqing Zou, Jimmy S Ren, Chunle Guo, and Chongyi Li. Dit4sr: Taming diffusion transformer for real-world image super-resolution. In *Proceedings of the IEEE/CVF International Conference on Computer Vision*, pages 18948–18958, 2025. 1
- [13] Patrick Esser, Sumith Kulal, Andreas Blattmann, Rahim Entezari, Jonas Müller, Harry Saini, Yam Levi, Dominik Lorenz, Axel Sauer, Frederic Boesel, et al. Scaling rectified flow transformers for high-resolution image synthesis. In *Forty-first international conference on machine learning*, 2024. 1, 3, 6
- [14] Samir Yitzhak Gadre, Gabriel Ilharco, Alex Fang, Jonathan Hayase, Georgios Smyrnis, Thao Nguyen, Ryan Marten, Mitchell Wortsman, Dhruva Ghosh, Jieyu Zhang, et al. Datacom: In search of the next generation of multimodal datasets. *Advances in Neural Information Processing Systems*, 36:27092–27112, 2023. 2
- [15] Peng Gao, Le Zhuo, Dongyang Liu, Ruoyi Du, Xu Luo, Longtian Qiu, Yuhang Zhang, Chen Lin, Rongjie Huang, Shijie Geng, Renrui Zhang, Junlin Xi, Wenqi Shao, Zhengkai Jiang, Tianshuo Yang, Weicai Ye, He Tong, Jingwen He, Yu Qiao, and Hongsheng Li. Lumina-t2x: Transforming text into any modality, resolution, and duration via flow-based large diffusion transformers, 2024. 1
- [16] Samar Khanna, Patrick Liu, Linqi Zhou, Chenlin Meng, Robin Rombach, Marshall Burke, David Lobell, and Stefano Ermon. Diffusionsat: A generative foundation model for satellite imagery. *arXiv preprint arXiv:2312.03606*, 2023. 3
- [17] Jang-Hyun Kim, Jinuk Kim, Seong Joon Oh, Sangdoon Yun, Hwanjun Song, Joonhyun Jeong, Jung-Woo Ha, and Hyun Oh Song. Dataset condensation via efficient synthetic-data parameterization. In *International Conference on Machine Learning*, pages 11102–11118. PMLR, 2022. 3
- [18] Vladimir Kulikov, Matan Kleiner, Inbar Huberman-Spiegelglas, and Tomer Michaeli. Flowedit: Inversion-free text-based editing using pre-trained flow models. In *Proceedings of the IEEE/CVF International Conference on Computer Vision*, pages 19721–19730, 2025. 1
- [19] Saehyung Lee, Sanghyuk Chun, Sangwon Jung, Sangdoon Yun, and Sungroh Yoon. Dataset condensation with contrastive signals. In *International Conference on Machine Learning*, pages 12352–12364. PMLR, 2022. 3
- [20] Kaiyu Li, Ruixun Liu, Xiangyong Cao, Xueru Bai, Feng Zhou, Deyu Meng, and Zhi Wang. Segearth-ov: Towards training-free open-vocabulary segmentation for remote sensing images. In *Proceedings of the Computer Vision and Pattern Recognition Conference*, pages 10545–10556, 2025. 1
- [21] Ming Li, Taojiannan Yang, Huafeng Kuang, Jie Wu, Zhaoning Wang, Xuefeng Xiao, and Chen Chen. Controlnet++: Improving conditional controls with efficient consistency feedback: Project page: liming-ai. github.io/controlnet_plus_plus. In *European Conference on Computer Vision*, pages 129–147. Springer, 2024. 1
- [22] Zhimin Li, Jianwei Zhang, Qin Lin, Jiangfeng Xiong, Yanxin Long, Xincheng Deng, Yingfang Zhang, Xingchao Liu, Minbin Huang, Zedong Xiao, et al. Hunyuan-dit: A powerful multi-resolution diffusion transformer with fine-grained chinese understanding. *arXiv preprint arXiv:2405.08748*, 2024. 1
- [23] Ziming Li, Han Wang, Yadian Wang, Gang Chen, Jing M. Chen, and Bin Chen. Large-scale high-resolution essential urban land cover category mapping using a semantic-augmented and noise-tolerant approach. *IEEE Transactions on Geoscience and Remote Sensing*, 63:1–21, 2025. 1

- [24] Yaron Lipman, Ricky TQ Chen, Heli Ben-Hamu, Maximilian Nickel, and Matt Le. Flow matching for generative modeling. *arXiv preprint arXiv:2210.02747*, 2022. 3, 5
- [25] Xingchao Liu, Chengyue Gong, and Qiang Liu. Flow straight and fast: Learning to generate and transfer data with rectified flow. *arXiv preprint arXiv:2209.03003*, 2022. 3, 5
- [26] MMSegmentation Contributors and open-mmlab. MM-Segmentation - OpenMMLab Semantic Segmentation Toolbox and Benchmark. <https://github.com/open-mmlab/mms Segmentation>, 2020. 6
- [27] Chong Mou, Xintao Wang, Liangbin Xie, Yanze Wu, Jian Zhang, Zhongang Qi, and Ying Shan. T2i-adapter: Learning adapters to dig out more controllable ability for text-to-image diffusion models. In *Proceedings of the AAAI conference on artificial intelligence*, pages 4296–4304, 2024. 3
- [28] Koichi Namekata, Amirmojtaba Sabour, Sanja Fidler, and Seung Wook Kim. Emerdiff: Emerging pixel-level semantic knowledge in diffusion models. In *The Twelfth International Conference on Learning Representations*, 2024. 1
- [29] Quang Nguyen, Truong Vu, Anh Tran, and Khoi Nguyen. Dataset diffusion: Diffusion-based synthetic data generation for pixel-level semantic segmentation. *Advances in Neural Information Processing Systems*, 36:76872–76892, 2023. 2, 3
- [30] Jiancheng Pan, Shiye Lei, Yuqian Fu, Jiahao Li, Yanxing Liu, Yuze Sun, Xiao He, Long Peng, Xiaomeng Huang, and Bo Zhao. Earthsynth: Generating informative earth observation with diffusion models. *arXiv preprint arXiv:2505.12108*, 2025. 1, 2, 3, 6, 7, 8
- [31] William Peebles and Saining Xie. Scalable diffusion models with transformers. In *Proceedings of the IEEE/CVF international conference on computer vision*, pages 4195–4205, 2023. 1
- [32] Bohao Peng, Jian Wang, Yuechen Zhang, Wenbo Li, Ming-Chang Yang, and Jiaya Jia. Controlnext: Powerful and efficient control for image and video generation. *arXiv preprint arXiv:2408.06070*, 2024. 1
- [33] Dustin Podell, Zion English, Kyle Lacey, Andreas Blattmann, Tim Dockhorn, Jonas Müller, Joe Penna, and Robin Rombach. Sdxl: Improving latent diffusion models for high-resolution image synthesis. *arXiv preprint arXiv:2307.01952*, 2023. 1
- [34] Ahmad Sajedi, Samir Khaki, Ehsan Amjadian, Lucy Z Liu, Yuri A Lawryshyn, and Konstantinos N Plataniotis. Datadam: Efficient dataset distillation with attention matching. In *Proceedings of the IEEE/CVF International Conference on Computer Vision*, pages 17097–17107, 2023. 3
- [35] Stability AI. Introducing Stable Diffusion 3.5, 2024. 1, 6, 7
- [36] Robin Strudel, Ricardo Garcia, Ivan Laptev, and Cordelia Schmid. Segmenter: Transformer for semantic segmentation. In *Proceedings of the IEEE/CVF international conference on computer vision*, pages 7262–7272, 2021. 2
- [37] Zhenxiong Tan, Songhua Liu, Xingyi Yang, Qiaochu Xue, and Xinchao Wang. Ominicontrol: Minimal and universal control for diffusion transformer. In *Proceedings of the IEEE/CVF International Conference on Computer Vision*, pages 14940–14950, 2025. 3
- [38] Datao Tang, Xiangyong Cao, Xuan Wu, Jialin Li, Jing Yao, Xueru Bai, Dongsheng Jiang, Yin Li, and Deyu Meng. Aerogen: Enhancing remote sensing object detection with diffusion-driven data generation. In *Proceedings of the Computer Vision and Pattern Recognition Conference*, pages 3614–3624, 2025. 1
- [39] Datao Tang, Hao Wang, Yudeng Xin, Hui Qiao, Dongsheng Jiang, Yin Li, Zhiheng Yu, and Xiangyong Cao. Terragen: A unified multi-task layout generation framework for remote sensing data augmentation. *arXiv preprint arXiv:2510.21391*, 2025. 1, 3
- [40] Hao Tang, Siyue Yu, Jian Pang, and Bingfeng Zhang. A training-free synthetic data selection method for semantic segmentation. In *Proceedings of the AAAI Conference on Artificial Intelligence*, pages 7229–7237, 2025. 2, 3, 7
- [41] Aysim Toker, Marvin Eisenberger, Daniel Cremers, and Laura Leal-Taixé. Satsynth: Augmenting image-mask pairs through diffusion models for aerial semantic segmentation. In *Proceedings of the IEEE/CVF Conference on Computer Vision and Pattern Recognition*, pages 27695–27705, 2024. 3
- [42] Haoxuan Wang, Jinlong Peng, Qingdong He, Hao Yang, Ying Jin, Jiafu Wu, Xiaobin Hu, Yanjie Pan, Zhenye Gan, Mingmin Chi, et al. Unicombine: Unified multi-conditional combination with diffusion transformer. *arXiv preprint arXiv:2503.09277*, 2025. 3
- [43] Junjue Wang, Zhuo Zheng, Ailong Ma, Xiaoyan Lu, and Yanfei Zhong. Loveda: A remote sensing land-cover dataset for domain adaptive semantic segmentation. *arXiv preprint arXiv:2110.08733*, 2021. 2, 6, 1
- [44] Shaobo Wang, Yicun Yang, Zhiyuan Liu, Chenghao Sun, Xuming Hu, Conghui He, and Linfeng Zhang. Dataset distillation with neural characteristic function: A minmax perspective. In *Proceedings of the Computer Vision and Pattern Recognition Conference*, pages 25570–25580, 2025. 3
- [45] Shaojin Wu, Mengqi Huang, Wenxu Wu, Yufeng Cheng, Fei Ding, and Qian He. Less-to-more generalization: Unlocking more controllability by in-context generation. *arXiv preprint arXiv:2504.02160*, 2025. 3
- [46] Yiming Xie, Varun Jampani, Lei Zhong, Deqing Sun, and Huaizu Jiang. Omnicontrol: Control any joint at any time for human motion generation. In *The Twelfth International Conference on Learning Representations*, 2024. 3
- [47] Han Xue, Zhiwu Huang, Qianru Sun, Li Song, and Wenjun Zhang. Freestyle layout-to-image synthesis. In *Proceedings of the IEEE/CVF conference on computer vision and pattern recognition*, pages 14256–14266, 2023. 6, 7, 1
- [48] Lihe Yang, Xiaogang Xu, Bingyi Kang, Yinghuan Shi, and Hengshuang Zhao. Freemask: Synthetic images with dense annotations make stronger segmentation models. *Advances in Neural Information Processing Systems*, 36:18659–18675, 2023. 2, 3, 6, 7, 8, 1
- [49] Ziqi Ye, Shuran Ma, Jie Yang, Xiaoyi Yang, Ziyang Gong, Xue Yang, and Haipeng Wang. Object fidelity diffusion for remote sensing image generation. *arXiv preprint arXiv:2508.10801*, 2025. 1
- [50] Sung-Hoon Yoon, Minghan Li, Gaspard Beaudouin, Congcong Wen, Muhammad Rafay Azhar, and Mengyu Wang.

- Splitflow: Flow decomposition for inversion-free text-to-image editing. *arXiv preprint arXiv:2510.25970*, 2025. 1
- [51] Shuai Yuan, Guancong Lin, Lixian Zhang, Runmin Dong, Jinxiao Zhang, Shuang Chen, Juepeng Zheng, Jie Wang, and Haohuan Fu. Fusu: A multi-temporal-source land use change segmentation dataset for fine-grained urban semantic understanding. *Advances in Neural Information Processing Systems*, 37:132417–132439, 2024. 2, 6
- [52] Hui Zhang, Dexiang Hong, Yitong Wang, Jie Shao, Xinglong Wu, Zuxuan Wu, and Yu-Gang Jiang. Creatilayout: Siamese multimodal diffusion transformer for creative layout-to-image generation. In *Proceedings of the IEEE/CVF International Conference on Computer Vision*, pages 18487–18497, 2025. 1, 3, 4
- [53] Lvmin Zhang, Anyi Rao, and Maneesh Agrawala. Adding conditional control to text-to-image diffusion models. In *Proceedings of the IEEE/CVF international conference on computer vision*, pages 3836–3847, 2023. 1, 3, 6
- [54] Yuxuan Zhang, Yirui Yuan, Yiren Song, Haofan Wang, and Jiaming Liu. Easycontrol: Adding efficient and flexible control for diffusion transformer. In *Proceedings of the IEEE/CVF International Conference on Computer Vision*, pages 19513–19524, 2025. 3
- [55] Chenbo Zhao, Yoshiki Ogawa, Shenglong Chen, Zhehui Yang, and Yoshihide Sekimoto. Label freedom: Stable diffusion for remote sensing image semantic segmentation data generation. In *2023 IEEE International Conference on Big Data (BigData)*, pages 1022–1030. IEEE, 2023. 7, 1
- [56] Hengshuang Zhao, Jianping Shi, Xiaojuan Qi, Xiaogang Wang, and Jiaya Jia. Pyramid scene parsing network. In *Proceedings of the IEEE conference on computer vision and pattern recognition*, pages 2881–2890, 2017. 7, 2
- [57] Shihao Zhao, Dongdong Chen, Yen-Chun Chen, Jianmin Bao, Shaozhe Hao, Lu Yuan, and Kwan-Yee K Wong. Uni-controlnet: All-in-one control to text-to-image diffusion models. *Advances in Neural Information Processing Systems*, 36:11127–11150, 2023. 1
- [58] Guangcong Zheng, Xianpan Zhou, Xuewei Li, Zhongang Qi, Ying Shan, and Xi Li. Layoutdiffusion: Controllable diffusion model for layout-to-image generation. In *Proceedings of the IEEE/CVF Conference on Computer Vision and Pattern Recognition*, pages 22490–22499, 2023. 3

Appendix

A. Differences Between CRFM and Inversion-Free Editing

Our control-rectify flow matching (CRFM) is designed to modulate the trajectory during the early RF process, guiding it toward the target conditional distribution and thereby improving the semantic alignment of the final generated images.

The concept of steering the rectified flow (RF) trajectory has also been similarly applied in image editing tasks. FlowEdit [18] modulates the trajectory of the RF by calculating the vector field difference between the source and target images at each time step. This approach obviates the need for latent inversion, and directly establishes the transition trajectory between the source and target images for image editing tasks. SplitFlow [50] further introduces a flow decomposition and aggregation framework, designed to address the inherent issues of gradient entanglement and semantic conflict within complex target prompts, which mitigates interference between attributes while maintaining overall semantic consistency.

The trajectories established by the aforementioned two methods represent a transformation process from the source data distribution $p_{\text{data}}^{\text{src}}$ to the target data distribution $p_{\text{data}}^{\text{tgt}}$. This process can be formally expressed in the form of the following ODE:

$$dz^{\text{edit}} = v_t^\Delta(z_t^{\text{src}}, z_t^{\text{tgt}})dt, \quad (14)$$

where z^{edit} denotes the latent state on the editing trajectory, while z_t^{src} and z_t^{tgt} represent the interpolated latent representations of the source and target states, respectively, at time $t \in [0, 1]$. Specifically, the velocity field difference $v_t^\Delta(z_t^{\text{src}}, z_t^{\text{tgt}})$ is defined as the subtraction of the source velocity field from the target velocity field, where $v(z_t, t)$ is the predicted velocity at latent state z_t and time t :

$$v_t^\Delta(z_t^{\text{src}}, z_t^{\text{tgt}}) = v(z_t^{\text{tgt}}, t) - v(z_t^{\text{src}}, t). \quad (15)$$

In contrast, our CRFM modulates the trajectory that connects the noise distribution $z_1 \sim \mathcal{N}(0, 1)$ to the conditional data distribution $z_0 \sim p(z_{\text{data}}|C^m)$ which is controlled by a semantic mask C^m . The probability path of this process can be constructed by solving the following ODE:

$$dz^{\text{ctrl}} = v_t^{\text{CRFM}}(z_t, t, C^m)dt, \quad (16)$$

where dz^{ctrl} is the latent state on the conditional trajectory. The term $v_t^{\text{CRFM}}(z_t, t, C^m)$ is the vector field adjusted by CRFM based on the semantic mask condition C^m at the current latent state z_t (at time t). CRFM vector field can be decomposed into two distinct components:

$$v_t^{\text{CRFM}}(z_t, t, C^m) = v_t(z_t, t, C^m) + v_t^{\text{rec}}(z_t, t, C^m). \quad (17)$$

Here, $v_t(z_t, t, C^m)$ represents the output vector field of RF model, conditioned on the semantic mask C^m and computed at the current latent state z_t and time t . $v_t^{\text{rec}}(z_t, t, C^m)$, is an estimated vector derived from the gradient, calculated using a Segmentation Network \mathcal{S} and the semantic mask C^m on the pre-synthesized image z_0^t of z_t . This component is formally defined as:

$$v_t^{\text{rec}}(z_t, t, C^m) \approx \alpha \nabla_v \mathcal{L}_{CE}(\mathcal{S}(z_0^t), C^m), \quad (18)$$

$$z_0^t = z_t - \sigma_t v_t(z_t, t, C^m), \quad (19)$$

where α is a manually set hyperparameter, σ_t is the schedule coefficient that governs the blend ratio between the noise and data during the forward process of RF. Furthermore, $\mathcal{L}_{CE}(\mathcal{S}(z_0^t), C^m)$ calculates the semantic loss between the output of the Segmentation Network $\mathcal{S}(z_0^t)$ and the semantic mask C^m .

Beyond these technical differences in trajectory construction, the core motivations of the two approaches are fundamentally distinct. FlowEdit and related editing methods are built on the principle that an effective editing algorithm should minimally alter the source image while faithfully transporting it toward the target distribution. Their objective is to construct a minimal and direct transition between $p_{\text{data}}^{\text{src}}$ to $p_{\text{data}}^{\text{tgt}}$.

In sharp contrast, CRFM aims to modulate the probability trajectory during the RF process for any initial state $z_1 \sim \mathcal{N}(0, 1)$, ensuring that the resulting generated state z_0 more closely aligns with the target data distribution $p(z_{\text{data}}|C^m)$.

B. Additional Experiment

B.1. Visualization of Comparative Results

We provide the visualization results of different methods on the LoveDA [43] dataset, including LabelFreedom [55], Freestyle [47], FreeMask [48], and EarthSynth [30], all of which are based on ControlNet [53]. As shown in Figure 3, the ControlNet architecture achieves stronger edge control because the feature outputs from its semantic mask control flow are directly added into the intermediate layers of the image diffusion branch via skip connections. This localized injection mechanism provides tight spatial conditioning.

In contrast, the MMDiT architecture processes the concatenated features of text and the semantic mask through a global Transformer-based attention mechanism. This architectural difference enables MMDiT to model long-range dependencies and better capture global context, thereby resulting in more natural and aesthetically pleasing generation and higher semantic consistency in complex scenes. By optimizing the vector field’s direction in the pixel-level latent space, CRFM significantly enhances the precision of

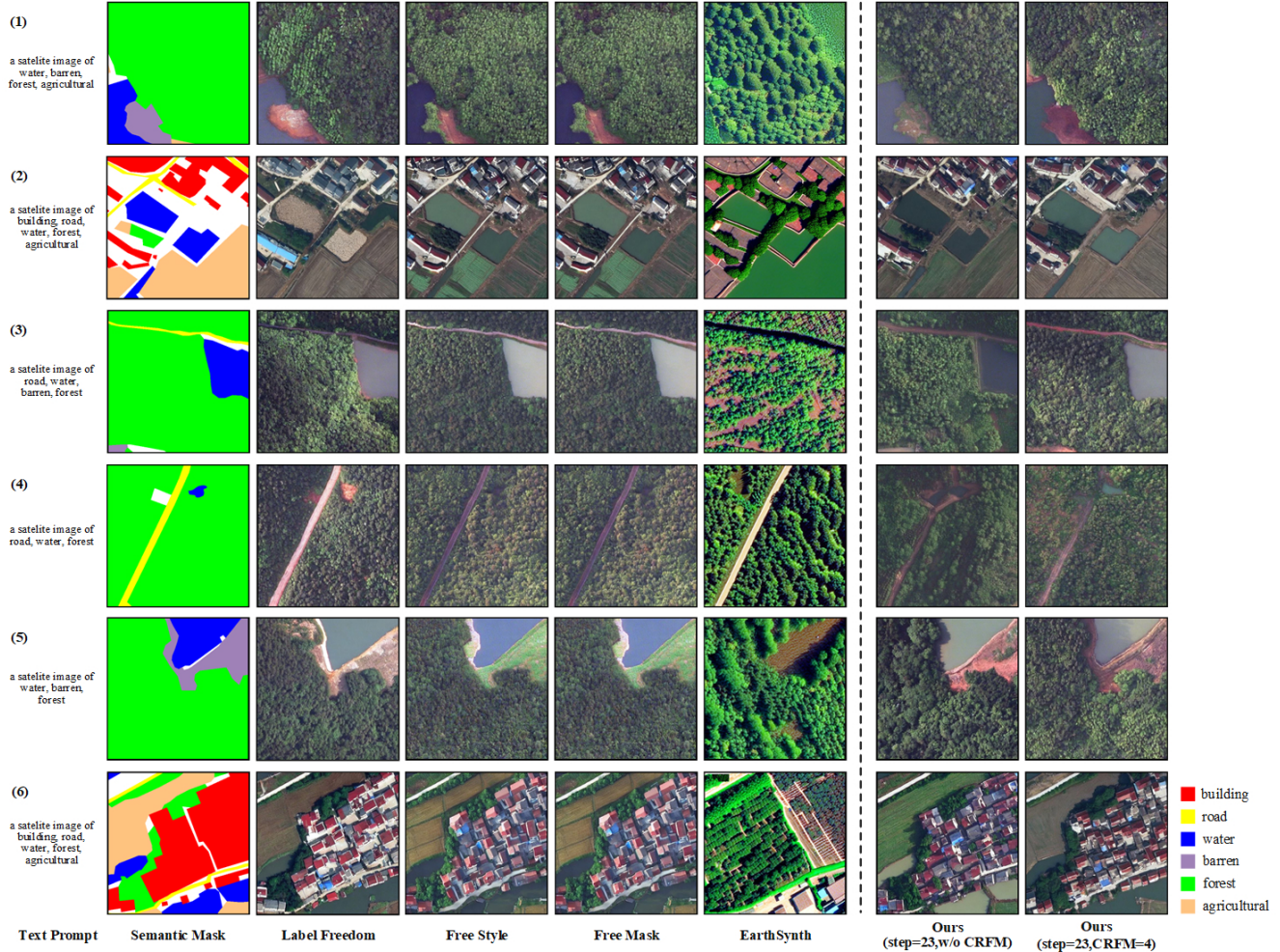


Figure 3. Qualitative comparison for mask-to-image generation by various methods.

Table 5. The performance of downstream tasks with varying pre-trained semantic segmentation models on CRFM.

Method	Seg. Model-1			Seg. Model-2			Seg. Model-3		
	OA	mIoU	mAcc	OA	mIoU	mAcc	OA	mIoU	mAcc
Pre-trained Seg. model (baseline)	74.27	45.27	56.44	69.11	40.76	52.98	67.98	30.12	40.48
Downstream task(step=18, CRFM=2)	75.86	47.99	59.46	75.11	47.30	59.89	75.07	46.35	58.64
Downstream task(step=18, CRFM=4)	76.24	48.93	60.54	75.46	48.35	60.82	75.47	47.65	60.19
Downstream task(step=18, CRFM=6)	76.02	49.57	62.19	75.66	48.92	61.14	75.58	48.44	60.67

edge control, thereby complementing the shortcomings of MMDiT in this regard.

B.2. Sensitivity Analysis of CRFM on Pre-Trained Semantic Segmentation Models

For the semantic segmentation model, we employ PSP-Net [56]. This choice is supported by the comparative analysis in TISynth [10], which evaluates architectures including PSPNet, Segmenter [36], and Mask2Former [7]. Their

findings indicates that CNN-based architectures demonstrate a superior performance advantage over transformer-based architectures for small datasets like FUSU-4k [51].

Because CRFM relies on the semantic segmentation model to compute the semantic loss between its prediction and the ground truth mask, the quality of the pre-trained model may directly affects CRFM performance. To verify the sensitivity of CRFM on pre-trained semantic segmen-

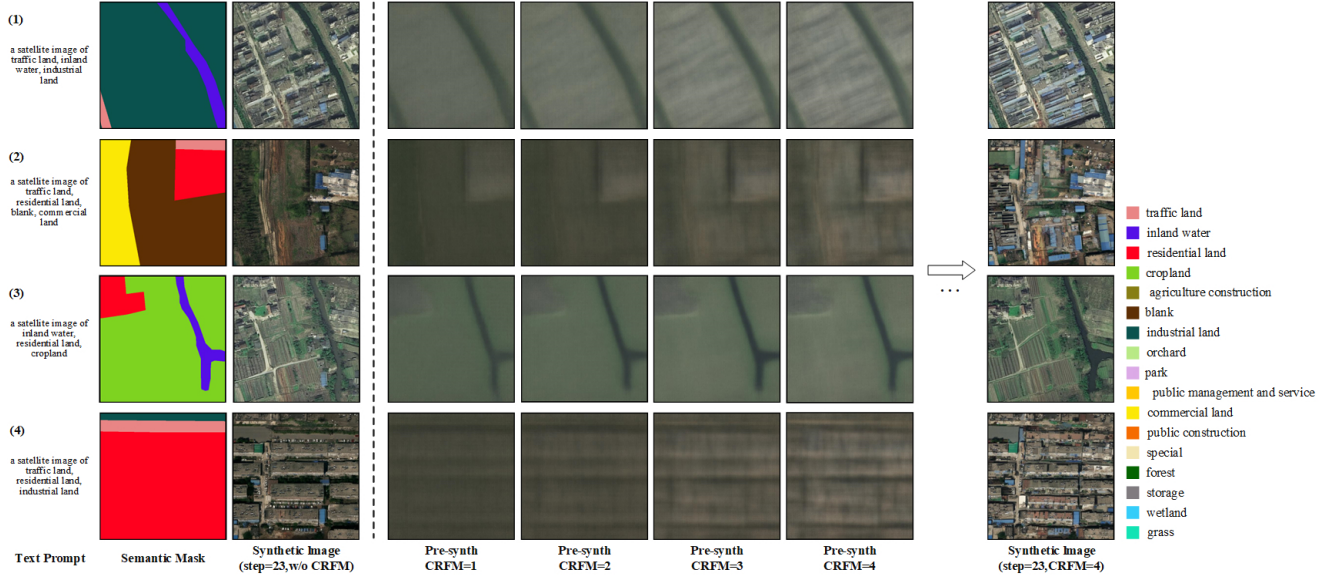


Figure 4. Visualization results of pre-synth images with different CRFM steps on the FUSU.

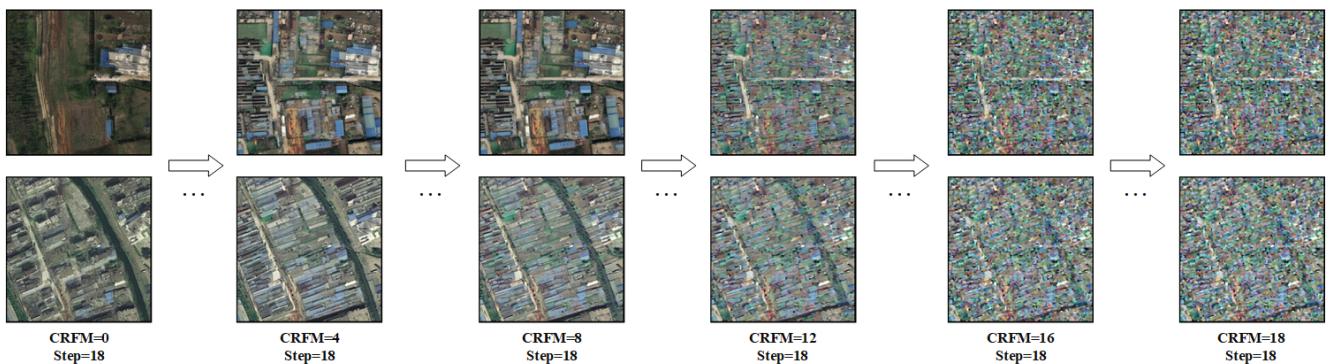


Figure 5. Visual comparison of generated samples with varying CRFM steps.

tation models, we design three segmentation models with different accuracies: Seg. Model-1 is trained on the full FUSU-4k dataset. Seg. Model-2 is trained on a 2k subset and Seg. Model-3 is trained on a 1k subset.

As shown in Table 5, we first report the performance of the pre-trained semantic segmentation models. Using these models as the evaluation modules within CRFM, we compare CRFM under different number of adjustment steps (i.e., 2, 4 and 6), while fixing the sampling step at 18. When utilizing lower-performing pre-trained models, the effectiveness of CRFM is slightly reduced. However, as the number of adjustment steps increases, the final performance consistently surpasses the baseline. This indicates that although the pre-trained semantic segmentation models vary in accuracy, they all possess a certain level of semantic discrimination capability. Such information is sufficiently reliable to guide and correct the sampling trajectory during the early sampling stage. Therefore, although CRFM is some-

what sensitive to the performance of the pre-trained segmentation model, this influence is limited because CRFM operates only in the early sampling stage. Consequently, it consistently delivers improvements over the baseline.

B.3. Analysis of Sampling with CRFM

To better understand the effect of CRFM on the flow trajectory, we visualize the pre-synth images generated by the CRFM algorithm during sampling, with the total sampling steps set to 18 and the number of CRFM adjustments set to 4. As shown in Figure 4, the generated pre-synth images increasingly align with the semantic structure of the ground-truth masks as the CRFM adjustments proceed. This indicates that CRFM is capable of adjusting the flow trajectory of the noise toward $p(z_{data}|C^m)$, a conclusion further supported by the comparison between generated images with and without CRFM.

However, we observe that setting the number of CRFM

adjustments excessively high—typically exceeding 50% of the total sampling steps leads to mode collapse. This phenomenon occurs because the generated images over-optimize to satisfy the pre-trained segmentation model’s perception, thereby resulting in a noticeable degradation of human-perceived visual quality. Figure 5 presents the visualization results for a total of 18 sampling steps, while varying the CRFM adjustment count from 0 to 18. A slight mode collapse appears at $\text{CRFM} = 8$, becomes severe at $\text{CRFM} = 12$, and when the CRFM frequency approaches the full sampling length, the outputs degenerate into adversarial-like samples that completely lose visual quality.